Oxygen Reduction Activity of Silk-derived Carbons

Tomoya Iwazaki[a,b], Hongsheng Yang[a], Ryoujin Obinata[a], Wataru Sugimoto[a],

Yoshio Takasu[a,*]

[a] Department of Fine Materials Engineering, Faculty of Textile Science and Technology, Shinshu University, 3-15-1 Tokida, Ueda, Nagano 386-8567, Japan

[b] Shinano Kenshi Co., Ltd., 1078 Kamimaruko, Ueda, Nagano 386-0498, Japan

*To whom correspondence should be addressed:

Tel: +81-268-21-5451, Fax: +81-268-21-5452, Email: ytakasu@shinshu-u.ac.jp.

Abstract

Carbonized silk fibroin (CS), which is free of metallic elements, showed high catalytic activity for oxygen-reduction reaction (ORR). The catalytic activity of CS for ORR was greatly enhanced by steam activation forming silk-derived activated carbon (CS-AC). The surface morphology, surface area, pore structure and remaining nitrogen species of the CSs were compared with those of the CS-ACs. The open-circuit potential and the power density of a polymer electrolyte fuel cell using a CS900-AC, which was heat-treated at 900°C prior to the steam activation, and a platinum/C (C: carbon black) anode under pure oxygen and hydrogen gases, respectively, both at 0.2 MPa, were 0.92 V and 142 mW cm^{-2} at 80°C. The ORR on the

activated carbon, CS900-AC, proceeded with a 3.5-electron reaction at 0.6 V (vs. RHE); however, this was improved to a 3.9-electron reaction with the addition of zirconium oxide at 20 wt% to CS900-AC. Durability test of the electrode was also performed in O_2-saturated $HClO_4$ solution.

Key words: cathode, catalyst, carbon, activated carbon, PEFC

1. Introduction

Silk, because of its superior properties of lightness, fineness, a pleasant feel, and a unique luster, has been used as a material for high-quality clothing since ancient times [1]. Raw silk consists of sericin and fibroin, the former of which is removed when silk is to be used as a fiber. The proteins that make up silk fibroin consist of 18 types of amino acid, such as glycine and alanine, all of which contain nitrogen atoms within their molecular structures. The silk fibroin can be carbonized by heat treatment under a flowing inert gas, and the surface area of the carbonized silk fibroin can be greatly increased by heating under flowing steam, a process known as steam activation [2]. Activated carbons are generally prepared from various kinds of organic materials, such as coconut or walnut shells, wood, bamboo, synthetic fibers, coal or oil. Unlike these activated carbons, the activated carbon prepared from silk fibroin contains a greater amount of nitrogen atoms within its carbon framework. We decided to investigate the

ORR activity of activated carbons since cheaper cathode catalysts must be developed if polymer electrolyte fuel cells (PEFCs) are to be widely adopted; platinum, which is currently widely used as a cathode catalyst in fuel cells, is expensive, scarce, and unstable.

In the previous paper, we reported that silk-derived activated carbons (CS-ACs) show high catalytic activity for the ORR both in sulfuric acid and as a PEFC [3]. Although the nitrogen atoms remaining in the carbon network seem to correlate with the ORR, the real role of the nitrogen atoms remains unclear, because the silk-derived activated carbon containing only 0.8% nitrogen in the carbon network showed considerably high activity for the ORR. A rotating ring disk electrode (RRDE) measurement suggested that the ORR on a silk-derived activated carbon electrode was equivalent to a 3.5-electron reaction.

Various kinds of carbon materials prepared by carbonization of nitrogen containing polymers, such as polyacrylonitrile, or metal complexes have been proposed as candidate cathode materials for the ORR, and are activated with metal salts or contain metal species themselves [4-11]. The most important feature of the CSs and CS-ACs is that they contain no metal species at all. If metal species were included in the cathode material, they would inevitably dissolve into the electrolyte on polarization. For example, Fe^{2+} ion forms the "Fenton reagent" with hydrogen peroxide, which is generated through the ORR, and hydroxyl radical attacks the polymer electrolyte membrane.

In this paper, the physical properties and catalytic activity of carbonized silk fibroin (CSs) are compared with those of activated carbons (CS-ACs) heat-treated at various temperatures prior to steam activation. In addition, we attempt to reduce the formation of H_2O_2 by oxide loading onto the activated carbon.

2. Experimental

2.1 Preparation of the samples

A *Bombyx mori* silk fibroin (Shinano Kenshi Co. Ltd., Japan) was used as the starting material after removing the sericin from the silk fiber [3]. Silk fibroin contains 18 different amino acids: glycine, alanine, valine, leucine, isoleucine, proline, tryptophan, phenylalanine, asparagine acid, glutamic acid, arginine, histidine, lysine, serine, threonine, tyrosine, methionine and cystine. The silk fibroin was carbonized under heat treatment at 500°C in a stream of N_2 gas for 6 h, giving a yield of 40%. The carbonized silk fibroin was ball-milled and then further heat-treated at 700, 900, 1200, and 1500°C under flowing N_2 gas for 3 h: the products are referred to as CS700, CS900, CS1200 and CS1500, respectively. Steam activation of the carbonized silk fibroins was performed at 850°C for 7 h. The total yield of the CS900-AC from the silk fibroin was 12%. The resulting activated carbon is denoted CS-AC, and the CS-AC which was heat-treated at 900°C prior to the steam activation is denoted as CS900-AC.

2.2 Characterization of the carbon samples

The physical properties of the CS and CS-AC samples were determined by using a high-resolution scanning electron microscope (HRSEM; Hitachi S-5000), a transmission electron microscope (TEM; JEOL JEM-2010), an x-ray diffractometer (XRD; Rigaku RINT-2550, with monochromated CuKα radiation at 40 kV and 40 mA), and an X-ray

photoelectron spectrometer (XPS; Shimazu AXIS ULTRA, with monochromated MgKα radiation at 15 kV and 10 mA; the binding energy of the spectra was corrected with reference to the C1s peak at 284.6 eV). The surface area was determined by the Brunauer–Emmett–Teller (BET) method with nitrogen gas as the adsorbate (BEL Japan, BELSORP28).

2.3 Electrochemical measurements for the ORR

The ORR activity of the powder specimens of CSs and CS-ACs was evaluated in 0.5 M H_2SO_4 solution at 60°C with a rotating disk electrode equipment (RDE; Nikko Keisoku Co., Ltd.; NDE). The Pyrex® glass cell has a carbon-fiber counter electrode, a hydrogen reference electrode, and a glassy-carbon working electrode (0.283 cm^2). A Luggin capillary was used to reduce the IR drop. The working electrode was prepared by the thin-film electrode method. Briefly, the powder specimen (20 mg) was dispersed in methanol (10 mL), and the suspension was ultra-sonicated for 30 min. Then, 10 μL of the resulting dispersion (20 μg of the catalyst powder) was dropped onto the polished glassy-carbon substrate, and the film was dried at 60°C. 10 μL of a 0.03 wt% dispersion of Nafion® ionomer (Aldrich) in a 5 wt% water/lower alcohol mixture was dropped onto the electrode surface to stabilize the catalyst on the glassy-carbon substrate, and the assembly was heated again to 60°C. All electrode potentials are referred to a reversible hydrogen electrode scale corrected for temperature effect [RHE(t)]. The acid solution was deaerated or saturated with oxygen by bubbling highly pure nitrogen or oxygen gas into the electrolytic solution for 40 min. Cyclic voltammograms (CVs) of the specimens were measured in both deaerated and O_2-saturated 0.5 M H_2SO_4 solutions. The onset potential for the ORR, E_{ORR}, which means the electrode potential where an additional cathodic current begins to be

observed on the voltammogram, was measured in the oxygen-saturated electrolyte compared to the cathodic current in the deaerated electrolyte during the cathodic potential sweep.

The selectivity of the CS-ACs was evaluated in 0.1 M $HClO_4$ solution at 30°C with a rotating ring disk electrode (RRDE; AUTOLAB PGSTAT 12). For the experiments, 300 mg of catalyst was dispersed into 10 mL of water/ethanol mixed solution, and 0.283 mg of catalyst dropped onto the glassy-carbon working electrode (0.283 cm^2). 10 μL of a 0.2 wt% dispersion of Nafion® ionomer (Aldrich) was dropped onto the working electrode to stabilize the catalyst. The collection coefficient of the ring electrode for the rotating ring disk electrode measurement was 0.349.

3. Results and Discussion

3.1 Physical properties of the CSs and CS-ACs

As shown in Fig. 1-(a), the CS was a few micrometers in size. The SEM images of CS samples heat treated at various temperatures showed no evidence of great differences so long as the observation was conducted by SEM. The macroscopic morphology of the CS-ACs was also the same as those of the CSs. Observations with HRSEM (Figs. 1 and 2) showed that the surface of the CS-ACs was flat at magnification. Even after the steam activation of CS-900 and CS1200 at 850°C for 7 h (CS900-AC and CS1200-AC), only a small change in the surface morphology was observed as is evident in the SEM images; however, the surface of the CS700-AC was somewhat rough, probably as a result of insufficient carbonization of the CS700.

The chemical compositions of both CSs and CS-ACs evaluated by XPS listed in Table 1 also support the insufficient carbonization of CS700. The contents of both nitrogen and oxygen species of CS700 were considerably decreased by heating to 900°C; i.e. CS900. A typical TEM image of the CS900-AC provides no evidence for the existence of a graphite-like phase (Fig. 2-(d)).

The specific surface areas of all the CSs were smaller than 10 m^2g^{-1} as listed in Table 2. On the other hand, those of CS-ACs were higher than that of the typical carbon black used for PEFCs (Vulcan XC-72R). The XRD patterns of CSs and CS-ACs shown in Fig. 3 suggest that graphitization of the CS-ACs increased gradually with increasing heat-treatment temperature. That is, the diffraction peak corresponding to (002) at $2\theta = 24°$ of the CS-ACs became slightly sharper (as evaluated from the half width of the (002) diffraction peaks) with increasing heat-treatment temperature, and the extent of the graphitization approached that of carbon black, although no definite structure was formed even when the CS was heat-treated at 1500°C.

3.2 Catalytic properties of the CSs and CS-ACs

Cyclic voltammograms in oxygen-saturated 0.5 M H_2SO_4 for the CSs which were heat-treated at various temperatures are shown in Fig. 4, and indicate that the catalytic activity for the ORR of the CS700 was the highest and drastically decreased with increasing heat-treatment temperature. The onset potential for the ORR, E_{ORR}, for CS700, CS900, CS1200 and CS1500 was respectively 0.70 V, 0.63 V, 0.55 V and 0.43 V vs. RHE. The steam activation of these carbonized silk fibroins, CSs, greatly enhances the catalytic activity for the ORR. The values of E_{ORR} for CS700-AC, CS900-AC and CR1200-AC were respectively 0.72 V, 0.84 V

and 0.81 V vs. RHE. The catalytic activity decreased in order of CS900-AC, CS1200-AC and CS700-AC.

One of the reasons why steam activation enhanced the catalytic activity is the increase in surface area: the specific surface area of each CS increased by 122–196 times as shown in Table 2. Although the resultant specific surface area decreased with heat-treatment temperature, the mesopore volume listed in Table 3 must also be considered, because mass transport in the mesopores is easier than in the micropores. The larger mesopore volume of CS1200-AC, 0.21 cm^3g^{-1}, than that of CS900-AC, 0.13 cm^3g^{-1}, seems to help retain the high catalytic activity of the catalyst in spite of the smaller surface area, as shown in Table 2, and lower nitrogen content, as shown in Table 1, compared to those of CS900-AC.

The catalytic activity of the porous electrode for the ORR in a sulfuric acid electrolyte is affected by various parameters such as: (1) the quality of active site, (2) the amount of effective active sites, or effective surface area of the electrode for the reaction, (3) reaction conditions such as type of electrolyte, temperature, concentration of reactant, or O_2, (4) conditions of test electrodes, and (5) polarization conditions. The first parameter (1) will be discussed in the following section.

3.3 Nitrogen species in the surface layers of the CSs and CS-ACs

With regard to the ORR on carbon electrodes, it has been proposed that nitrogen atoms in the carbon participate directly or indirectly in the reaction. As has been proposed by many investigators, various types of nitrogen atoms, including pyridine-like nitrogen (398.6 eV), pyrrole-like nitrogen (400.5 eV), quaternary nitrogen (401.3 eV), and pyridine-like oxide

nitrogen (402–405 eV), have been observed as described in our previous paper for the CS-ACs as well as in nitrogen-containing carbons [12-16]. In the case of CSs (Fig. 6), the proportion of pyridine-like N species decreased with increasing heat-treatment temperature, and almost disappeared for CS1200, whereas some quaternary nitrogen (401.3 eV) species remained even after the heat treatment at 1200°C. On the N1s XPS spectrum of the CS1500 no evident peak was found except a trace peak appearing between 401 eV and 402 eV. The distribution of the peak areas of these four N1s peaks of CSs and CS-ACs are listed in Table 4. A comparison of the effects of heat-treatment temperature on the distribution of the four nitrogen species of CSs with that of the CS-ACs suggests that no selective elimination of any specific nitrogen species resulted in steam activation of the CSs.

Various methods of introducing nitrogen into carbon materials to enhance their catalytic activity on the ORR have been attempted. Techniques for nitrogen doping of carbon materials can be divided into two categories [17]: doping directly during the synthesis of the porous carbon material and post-treatment of pre-synthesized carbon materials with a nitrogen-containing precursor, e.g. NH_3. The former, which are often used for the preparation of nitrogen-doped carbon nanotubes and nanofibers, include techniques such as: various types of chemical vapor deposition, pyrolysis of nitrogen-containing metal complexes [18-23], a resin with ligand [7], a poly-alcohol with a complex and/or melamine, and polyaniline with metal salts. An example of the latter category is the doping of pristine activated carbons or carbon nanomaterials under treatment of NH_3 at high temperature [24] (600–900°C). Attempts to introduce nitrogen atoms into carbon nanostructures and their composites have shown some potential for use in the production of PEFC catalysts.

This investigation showed that quaternary nitrogen atoms are a major contributor to the ORR (Fig. 6). The activated carbon is heat-resistant; i.e. it showed a high catalytic activity for the ORR even after heat treatment at 1200°C. This was the case even though most nitrogen-containing carbon materials are prepared at temperatures below 1100°C. This should guarantee the durability of the carbon materials, because the greater the extent of graphitization of the carbon material, the greater the durability should be. Since large quantities of unused silk are produced by the textile industry, silk-derived activated carbon, which is free of metallic elements, is inexpensive.

It has been suggested that using nitrogen-doped carbon as a catalyst support should improve the durability of the resultant catalysts due to enhanced π bonding and basicity resulting from the strong electron-donor behavior of nitrogen [25-29]. Actually, however, the N-doped layer showed a higher conductivity than the undoped one, probably because of the nature of n-type doping and the strong electron-donor states near the Fermi level. This is further confirmed by quantum chemical calculations [30]. Therefore, silk-derived activated carbon could potentially be used not only as a cathode catalyst itself, but also as an "active support" that contributes directly to the ORR for a catalyst.

3.4 Performance of a PEFC with a CS-AC

Figure 7 shows the polarization curve at 80°C for a polymer electrolyte fuel cell (PEFC) with a membrane electrode assembly (MEA) constructed with a Pt (0.1 mg cm^{-2})/C catalyst anode, a perfluorosulfonic acid membrane (20 μm in thickness), and a cathode comprising

CS1200-AC (8.4 mg cm^{-2}) mixed with a perfluorosulfonic acid ionomer. Pure hydrogen and oxygen were introduced at a gauge pressure of 0.2 MPa for the anode and cathode, respectively. The cell performance was markedly dependent on the amount of CS1200-AC that was used. Since the performance of a typical PEFC using a Pt/C cathode is considerably greater than that of this cell, the catalytic activity of silk-derived activated carbon must be enhanced much more if it is to be used for the cathode catalyst of practical PEFC cells. It must be noted that this high performance was attained with a cathode containing no metal elements at all.

3.5 Addition of zirconium oxide to a CS-AC electrode

Two mechanisms have been proposed for the ORR: the first is a 4-electron reaction: $O_2 + 4H^+ + 4\ e^- \rightarrow 2\ H_2O$ and the second is a 2-electron reaction [31]: $O_2 + 2\ H^+ + 2\ e^- \rightarrow H_2O_2$. Although the usual reaction that occurs on graphite electrodes is nearly always the two-electron reaction, there have been reports that reactions involving more electrons may take place on nitrogen-containing carbon electrodes [11, 17-20, 24]. Analyses of the ORR by a method involving a rotating ring disk electrode showed that the ORR on CS900-AC proceeds by a 3.5-electron reaction at 0.6 V vs. RHE, for example Fig. 8-(a) and Fig. 9-(a); however, the addition of zirconium oxide particles with a diameter of less than 100 nm to the CS900-AC resulted in a 3.9-electron reaction for the ORR as shown in Fig. 8-(b) and Fig. 9-(b). Since zirconium oxide shows catalytic activity for the ORR [32], the added ZrO_2 particles must contribute to the reduction of H_2O_2 into H_2O not the oxidation of H_2O_2.

In this paper, the average number of electrons transferred, *n*, was calculated by the following equation:

$$n = 4\, I_D / \{I_D + (I_R/N)\} \qquad (1),$$

where, I_D is the current at the disk, I_R the current at the ring and N the experimental collection efficiency which corresponds to the I_R/I_D ratio (N = 0.349), determined using an aqueous solution containing 1 mM $K_3[Fe(CN)_6]$ and 0.1 M K_2SO_4.

3.6 Durability of the silk-derived activated carbon electrode

A durability test of the CS900-AC activated carbon was carried out by cyclic voltammetry in O_2-saturated 0.1 M $HClO_4$ at 30°C, where repeated potential sweeps between 0.1 and 1.2 V vs. RHE at 100 mV s^{-1} in a stationary state, were performed. Figure 10 shows the cyclic voltammograms at various potential sweeps; 1, 10, 100, 200, 500, 1000, 2000 and 6000 cycles. Only a little change in the voltammetric charge between 1.0 V and 1.1 V vs. RHE after 6000 cycles of the potential sweep, presented in Fig. 11, shows that the consumption of the carbon material by the potential cycles in O_2-saturated solution was not serious. In Fig. 12, the dependence of the current density for the ORR on the potential cycles is presented which was evaluated from the cyclic voltammograms shown in Fig. 10. As shown in this figure, little decay of the catalytic activity with the potential cycles was observed beyond the 1000 cycles.

4. Conclusion

Carbonized silk fibroin showed high catalytic activity for the ORR in a sulfuric acid solution. The catalytic activity of CS for the ORR decreased drastically with increasing heat-treatment temperature from 700°C to 1500°C. The steam activation of the carbonized silk fibroin at 850°C greatly enhanced the catalytic activity. The enhancement of the catalytic activity is thought to be

caused by the more than 100-fold enlargement of the surface area; however, the increase in mesopore volume by the treatment seems to effectively enhance catalytic activity. Although four types of nitrogen species were found in the surface layers of both carbonized silk fibroins and the steam-activated ones (silk-derived activated carbons), quaternary nitrogen seems to be the most important species for the ORR. As the active site for the ORR on the activated carbon, the following candidates are suggested: (1) the quaternary nitrogen atoms, (2) the nearest-neighbor carbon atoms surrounding the quaternary nitrogen atoms, (3) the vacancies of the quaternary nitrogen atoms, and (4) the nearest-neighbor carbon atoms of the vacancies of the quaternary nitrogen atoms. The open-circuit potential and the power density of a polymer electrolyte fuel cell using the most active silk-derived activated carbon, CS900-AC, which was heat-treated at 900°C prior to the steam activation, and a platinum/carbon black anode under pure oxygen and hydrogen gases, respectively, both at 0.2 MPa, were 0.92 V and 142 mW cm^{-2} at 80°C. Although the ORR on the activated carbon, CS900-AC, proceeded with a 3.5-electron reaction at 0.6 V (vs. RHE), it was improved to a 3.9-electron reaction by the addition of zirconium oxide particles at 20 wt% of the silk-derived activated carbon. Except for the initial stage of the polarization, not only high durability but also well stability in the catalytic activity of the activated carbon in an O_2-saturated electrolyte was confirmed. Since the performance of the PEFC using the silk-derived activated carbon is still not high enough, the catalytic activity of silk-derived activated carbon must be greatly enhanced before it can be applied to practical PEFC cells.

Note that the silk-derived activated carbon, which contains no metallic species by nature and graphite-like phase, shows considerably high catalytic activity for the ORR. That is, the highest

onset potential for the ORR, E_{ORR}, was 0.84 V vs. RHE at 60°C, and a PEFC using activated carbon as the cathode achieved a power density of 142 mW cm^{-2} at 80°C.

Acknowledgments

This work was supported in part by the "Polymer Electrolyte Fuel Cell Program – Development of Next Generation Technology" from the New Energy and Industrial Technology Development Organization (NEDO) of Japan.

References

[1] G. Chen, J. Guan, T. Xing, X. Zhou, J. Appl. Polym. Sci. 102 (2006) 424.

[2] Y. J. Kim, Y. Abe, T. Yanagiura, K. C. Park, M.Shimizu, T. Iwazaki, S. Nakagawa, M. Endo, M. S. Dresselhaus , Carbon 45 (2007) 2116.

[3] T. Iwazaki, R. Obinata, W. Sugimoto, Y. Takasu, Electrochem. Commun. 11 (2009) 376.

[4] R. Jasinski, Nature 201 (1964) 1212.

[5] H. Jahnke, M. Schönborn, G. Zimmermann, Topics in Current Chemistry 61 (1976) 133.

[6] S. Gupta, D. Tryk, I. Bae, W. Aldred, E. Yeager, J. Appl. Electrochem., 19 (1989) 19.

[7] J. Ozaki, S. Tanifuji, N. Kimura, A. Furuichi, A. Oya, Carbon 44 (2006) 1324.

[8] L. Zhang, J. J. Zhang, D.P. Wolkinson, H.J. Wang, J. Power Sources, 156 (2006) 171.

[9] P. H. Matter, E. Wang, M. Arias, E.J. Biddinger, O.U. Ozkan, J. Phys. Chem. B, 110 (2006) 18374.

[10] R. Bashyan, P. Zelenay, Nature 443 (2006) 63-69.

[11] J. Ozaki, S. Kimura, T. Anahara, A. Oya, Carbon 45 (2007) 1847.

[12] K. Staczyk, R. Dziembaj, Z. Piwowarska, S. Witkowski, Carbon 33 (1995) 1383.

[13] J. R. Pels, F. Kapteijn, J. A. Moulijn, Q. Zhu, K. M. Thomas, Carbon 33 (1995) 1641.

[14] J. Casanovas, J. M. Ricart, J. Rubio, F. Illas, J. M. Jiménez-Mateos, J. Am. Chem. Soc. 118 (1996) 8071.

[15] J. M. J. Mateos, J. L. G. Fierro, Surf. Interface Anal. 24 (1996) 223.

[16] E. Raymundo-Piñero, D. Cazorla-Amorós, A. Linares-Solano, J. Find, U. Wild, R. Schlögl, Carbon 40 (2002) 597.

[17] Y. Shao, et al., Applied Catalysis B: Environmental, 79 (2008) 89.

[18] P. H. Matter, E. Wang, M. Arias, E. J. Biddinger, U. S. Ozkan, J. Mol. Catal. A: Chem. 246 (2007) 73.

[19] P. H. Matter, U. S. Ozkan, Catal. Lett. 109(2006) 115.

[20] P. H. Matter, E. Wang, M. Arias, E. J. Biddinger, U. S. Ozkan, J. Phys. Chem. B 110 (2006) 18374.

[21] S. Maldonado, K. J. Stevenson, J. Phys. Chem. B 109 (2005) 4707.

[22] P. H. Matter, E. Wang, U. S. Ozkan, J. Catal. 243 (2006) 395.

[23] P. H. Matter, L. Zhang, U. S. Ozkan , J. Catal. 239(2006) 83.

[24] R. A. Sidik, A. B. Anderson, N. P. Subramanian S. P. Kumaraguru, B. N. Popov, J. Phys. Chem. B 110 (2006) 1787.

[25] V. V. Strelko, V. S. Kuts, P. A. Thrower, Carbon 38 (2000) 1499.

[26] F. Colomam, A. Sepulvedaescribano, F. Rodriguezreinoso, J. Catal. 154 (1995) 299.

[27] S. Maldonado, K. J. Stevenson, J. Phys. Chem. B 109 (2005) 4707.

[28] S. van Dommele, K. P. de Jong, J. H. Bitter, Chem. Commun. 4859 (2006) 4861.

[29] A. C. M. Carvalho, M. C. dos Santos, J. Appl. Phys. 100 (2006) 084305.

[30] T. Ikeda, M. Boero, S. F. Huang, K. Terakura, M. Oshima, J. Ozaki, J. Phys. Chem. C 112 (2008) 14706.

[31] E. Jeager, Electrochim. Acta 29 (1984) 1527.

[32] Y. Liu, A. Ishihara, S. Mitsushima, N. Kamiya, K.-I. Ota, Electrochem. Solid-State Lett., 8 (2005) A400.

Figure captions

Figure 1 SEM images of the carbonized silk fibroins heat-treated at various temperatures: (a) CS700 (low magnification), (b) CS700, (c) CS900 and (d) CS1200.

Figure 2 SEM images of the silk-derived activated carbons: (a) CS700-AC, (b) CS900-AC, (c) CS1200-AC and a TEM image of CS900-AC.

Figure 3 X-ray diffraction patterns of (a) CS700, (b) CS900, (c) CS1200, (d) CS1500, (e) carbon black (Vulcan XC-72R; CB), (f) CS700-AC, (g) CS900-AC and (h) CS1200-AC.

Figure 4 Cyclic voltammograms of (a) CS700, (b) CS900, (c) CS1200 and (d) CS1500 in 0.5 M H_2SO_4 at 60ºC. The potential sweep rate was 10 mV s^{-1}. Black lines: at 0 rpm in 0.5 M H_2SO_4 deaerated with N_2, Red lines: at 2000 rpm in 0.5 M H_2SO_4 saturated with O_2.

Figure 5 Cyclic voltammograms of (a) CS700-AC, (b) CS900-AC, (c) CS1200-AC and (d) Vulcan CB in 0.5 M H_2SO_4 at 60ºC. The potential sweep rate was 10 mV s^{-1}. Black lines: at 0 rpm in 0.5 M H_2SO_4 deaerated with N_2, Red lines: at 2000 rpm in 0.5 M H_2SO_4 saturated with O_2.

Figure 6 X-ray photoelectron spectra of the various carbon materials: (a) CS700, (b) CS900, (c) CR1200, (d) CS1500, (e) CS700-AC, (f) CS900-AC, (g) CR1200-AC and (h) CB. The black lines are the raw spectra; the red, green, blue, and pink lines correspond to pyridine-like N (398.6 eV), pyrrole-like N (400.5 eV), quaternary N (401.3 eV), and pyridine-like oxide N (402–405 eV), respectively. The atomic percent and atomic ratios of these specimens are listed in Table 2.

Figure 7 The polarization curve, recorded at 80ºC by using a membrane-electrode assembly (MEA), for a polymer electrolyte fuel cell (PEFC) comprising a Pt/C catalyst anode, a perfluorosulfonic acid membrane (20 μm in thickness), and a cathode comprising CS900-AC (loading 8.4 mg cm^{-2} geometric surface area) mixed with a perfluorosulfonic acid ionomer. Pure hydrogen and pure oxygen were introduced at a pressure of 0.2 MPa to the anode and cathode, respectively.

Fig. 8 Voltammograms of (a) CS900-AC and (b) CS900-AC loading 20 mass% of the ZrO_2 electrodes for the ORR measured in oxygen-saturated 0.1 M $HClO_4$ at 30ºC by the RRDE method at 2000 rpm. The ring current was adjusted with the collection coefficient of 0.349 of

this measurement system.

Fig. 9 Average number of electrons transferred (*n*) during ORR on (a) CS900-AC and (b) CS900-AC loading 20 mass% of the ZrO_2 electrodes for the ORR measured in oxygen-saturated 0.1 M $HClO_4$ at 30ºC by the RRDE method at 2000 rpm.

Fig. 10 Cyclic voltammograms of CS900-AC in O_2-saturated 0.1 M $HClO_4$ solution at 30 ºC in a stationary state to evaluate the durability of the activated carbon.

Loading amount of the activated carbon 1.0 mg cm^{-2}. Potential sweep rate: 100 mV s^{-1}.

(a) : the cyclic voltammogram in a deaerated 0.1 M $HClO_4$ solution with N_2 before the durability test carried out in O_2-saturated 0.1 M $HClO_4$ solution. (b), (c), (d), (e), (f), (g), (h), and (i) : the cyclic voltammograms measured in O_2-saturated 0.1 M $HClO_4$ solution after 1, 10, 100, 200, 500, 1000, 2000 and 6000 potential cycles, respectively.

Fig. 11 Capacitance variation of CS900-AC with the number of cycles.

Potential range used for the determination of the capacitance in deaerated 0.1 M $HClO_4$ before the durability test and in O_2-saturated solution of the electrode was 1.0 V~1.1 V vs. RHE.

Fig. 12 Dependence of the current density for the ORR at 0.7 V vs. RHE on the potential cycles evaluated from the cyclic voltammograms shown in Fig. 10.

Table 1 Atomic content and atomic ratios of CSs, CS-ACs and a typical carbon black evaluated by XPS

Sample	surface atomic content			atomic ratios		
	C1s	N 1s	O1s	N/C [a)]	O/C	N/C [b)]
CS700	86.5	7.5	6.0	0.087	0.069	0.170
CS900	92.4	2.8	4.8	0.030	0.052	0.069
CS1200	94.7	1.1	4.2	0.012	0.044	0.020
CS700-AC	83.9	3.6	12.5	0.043	0.149	0.063
CS900-AC	91.0	6.0	3.0	0.066	0.033	0.059
CS1200-AC	97.1	0.7	2.2	0.007	0.023	0.012
CB	95.9	0	3.8	0	0.040	

CB: Vulcan carbon black XC-72R

a) Determined by XPS

b) Determined by elemental analysis

Table 2 Specific surface area of CSs, CS-ACs and a typical carbon black determined by BET method

Sample	specific surface area m^2g^{-1}	Sample	specific surface area m^2g^{-1}
CS700	8.3	CS700-AC	1018
CS900	3.0	CS900-AC	588
CS1200	3.4	CS1200-AC	464
		CB	220

The data of CS700-AC, CS900-AC, CS1200-AC and CB were cited from Ref. 3.

Table 3 Micro- and mesopore volumes of CSs, CS-ACs and a typical carbon black

Sample	Micropore volume cm^3g^{-1}	Mesopore volume cm^3g^{-1}
CS700-AC	0.43	0.12
CS900-AC	0.24	0.13
CS1200-AC	0.25	0.21
CB	0.07	0.31

Table 4 Distribution of N species obtained from the deconvolution of the N1s peaks by XPS

Sample	N/C	Pyridine-like 398.6 eV	Pyrrrole-like 400.5eV	Quaternary 401.3 eV	Pyridine-like Oxide 402-405 eV
CS700	0.087	0.030	0.007	0.038	0.012
CS900	0.030	0.010	0.003	0.012	0.006
CS1200	0.012	0	0	0.009	0.002
CS700-AC	0.043	0.016	0.003	0.017	0.006
CS900-AC	0.066	0.019	0.003	0.039	0.005
CS1200-AC	0.007	0	0	0.006	0.001

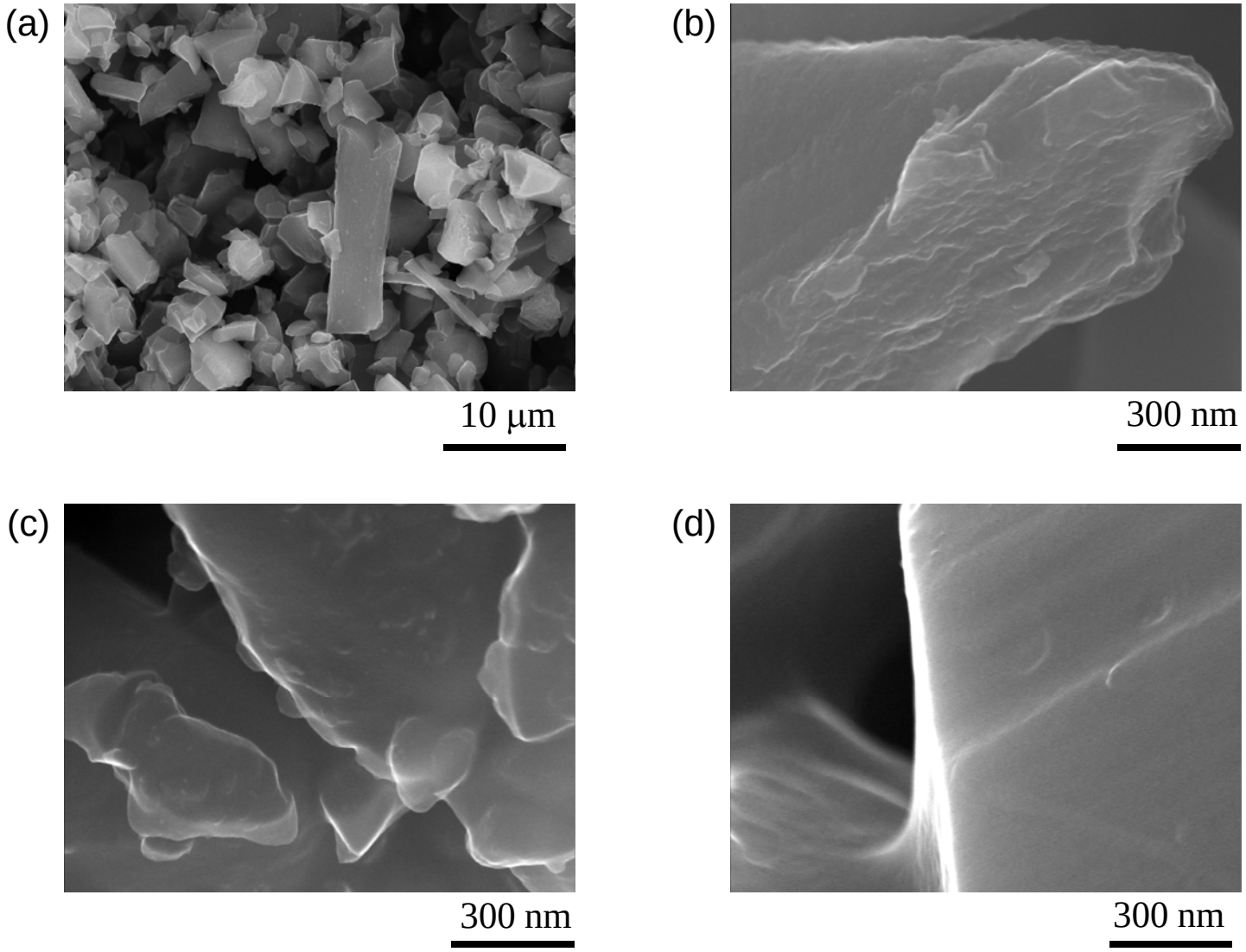

T. Iwazaki et al., Fig. 1

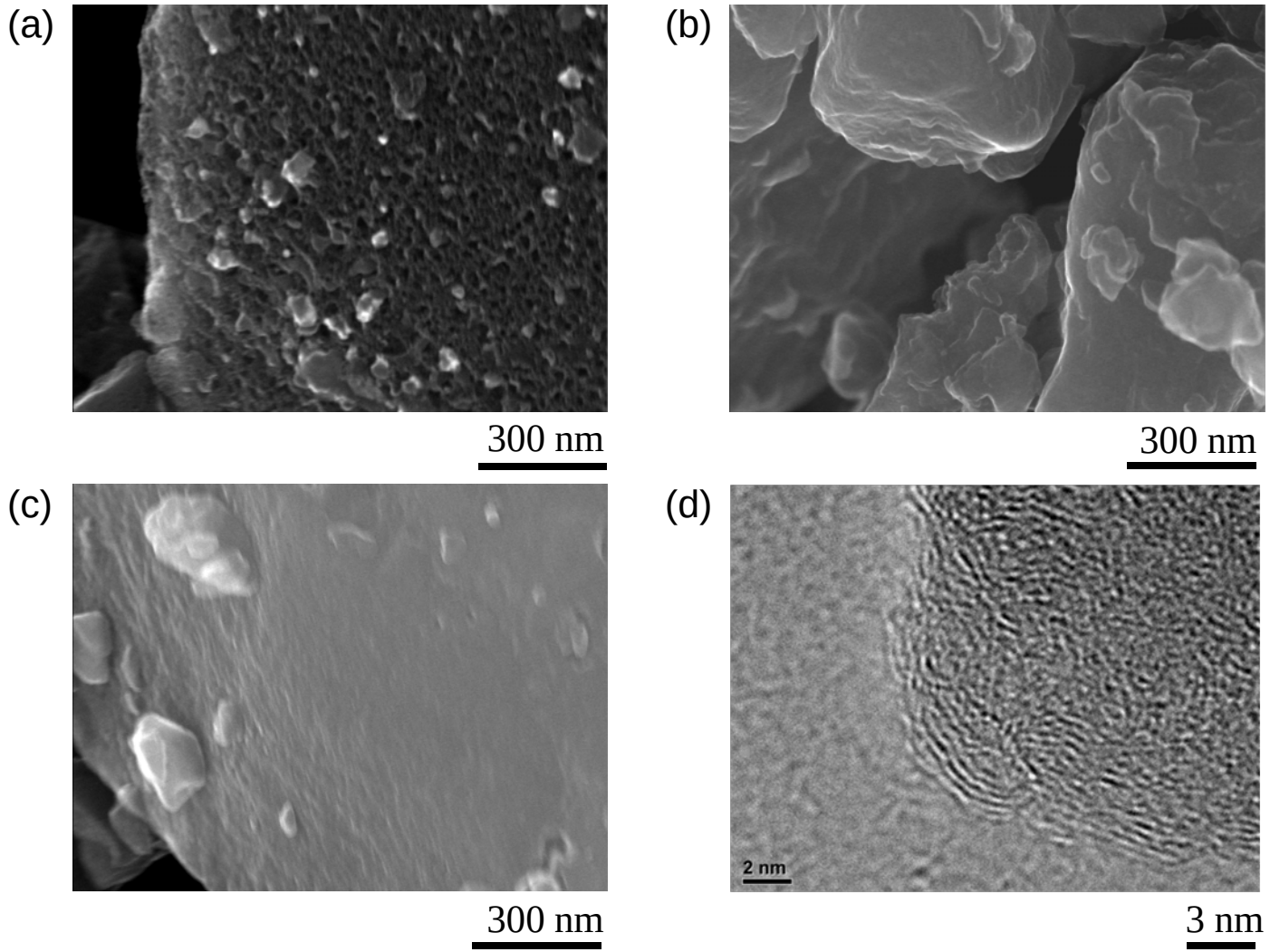

T. Iwazaki et al., Fig. 2

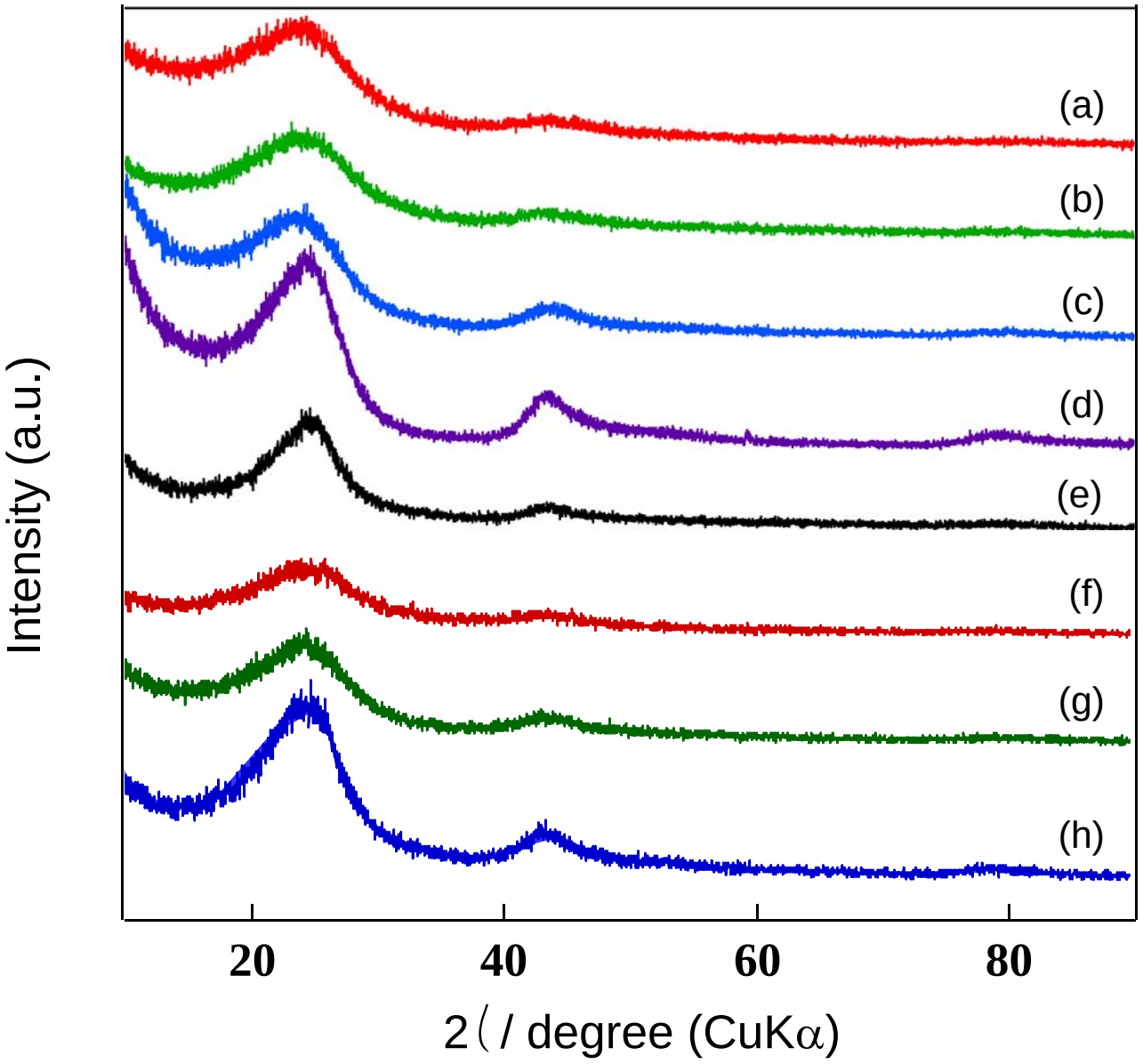

T. Iwazaki et al., Fig. 3

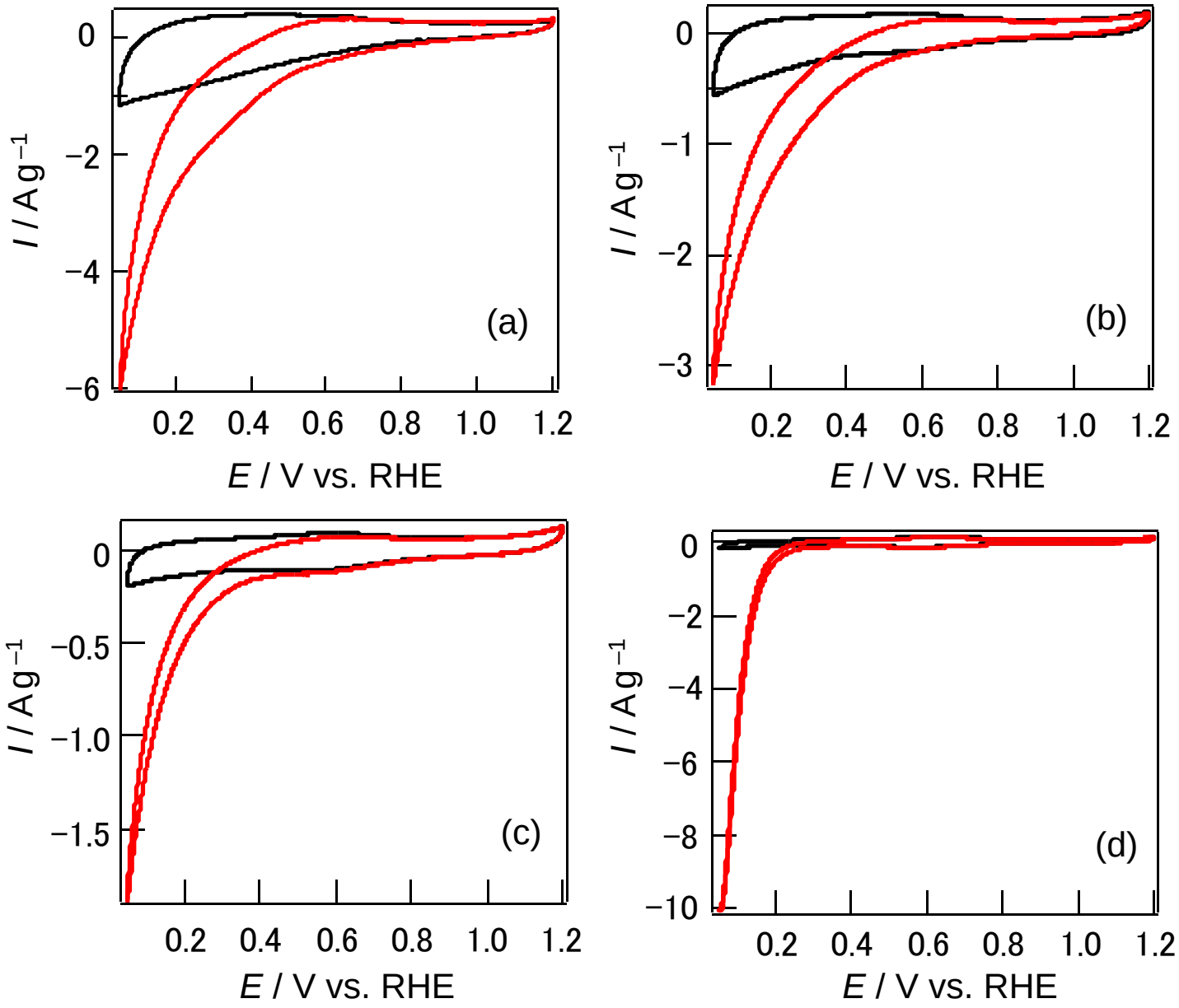

T. Iwazaki et al., Fig. 4

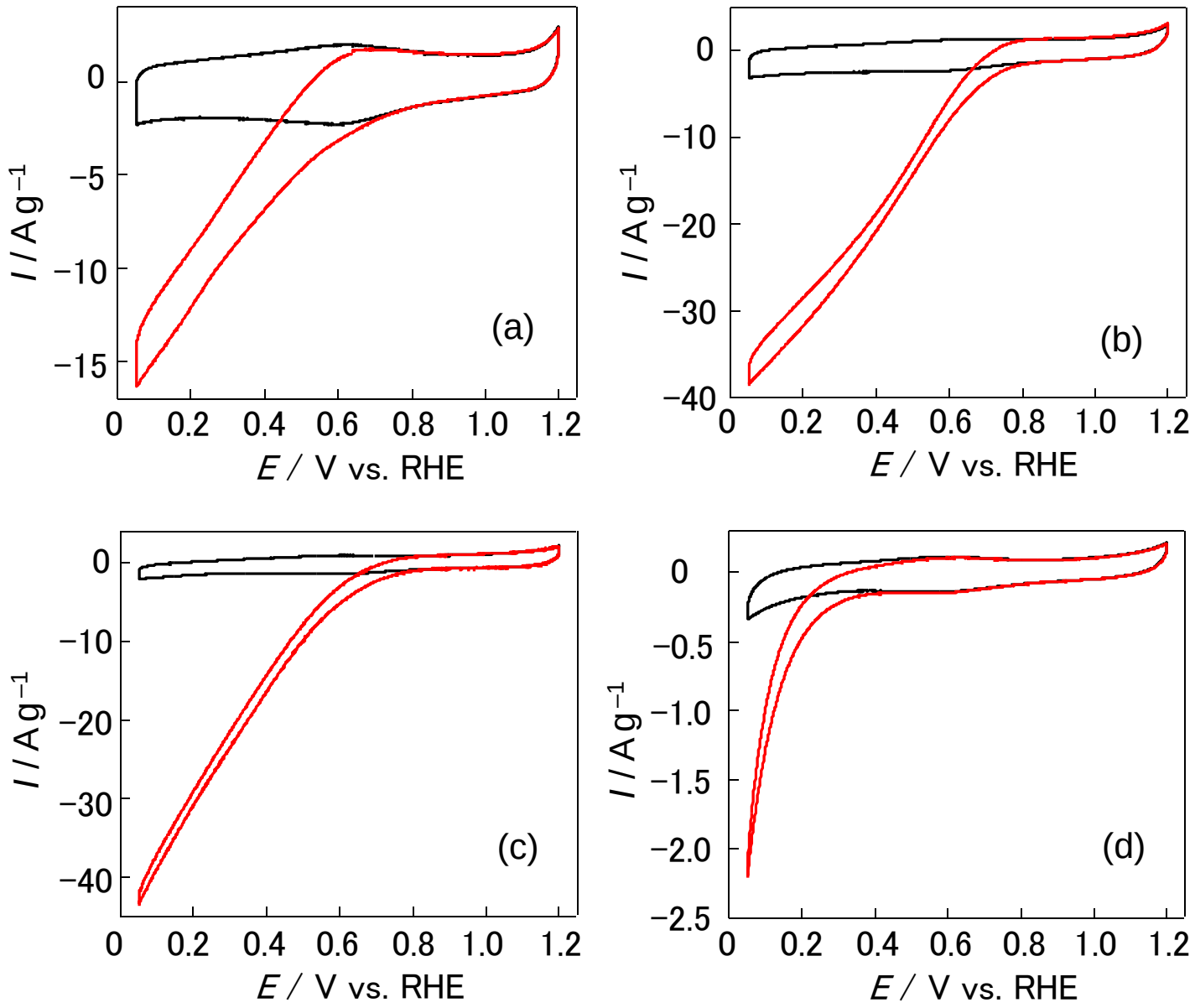

T. Iwazaki et al., Fig. 5

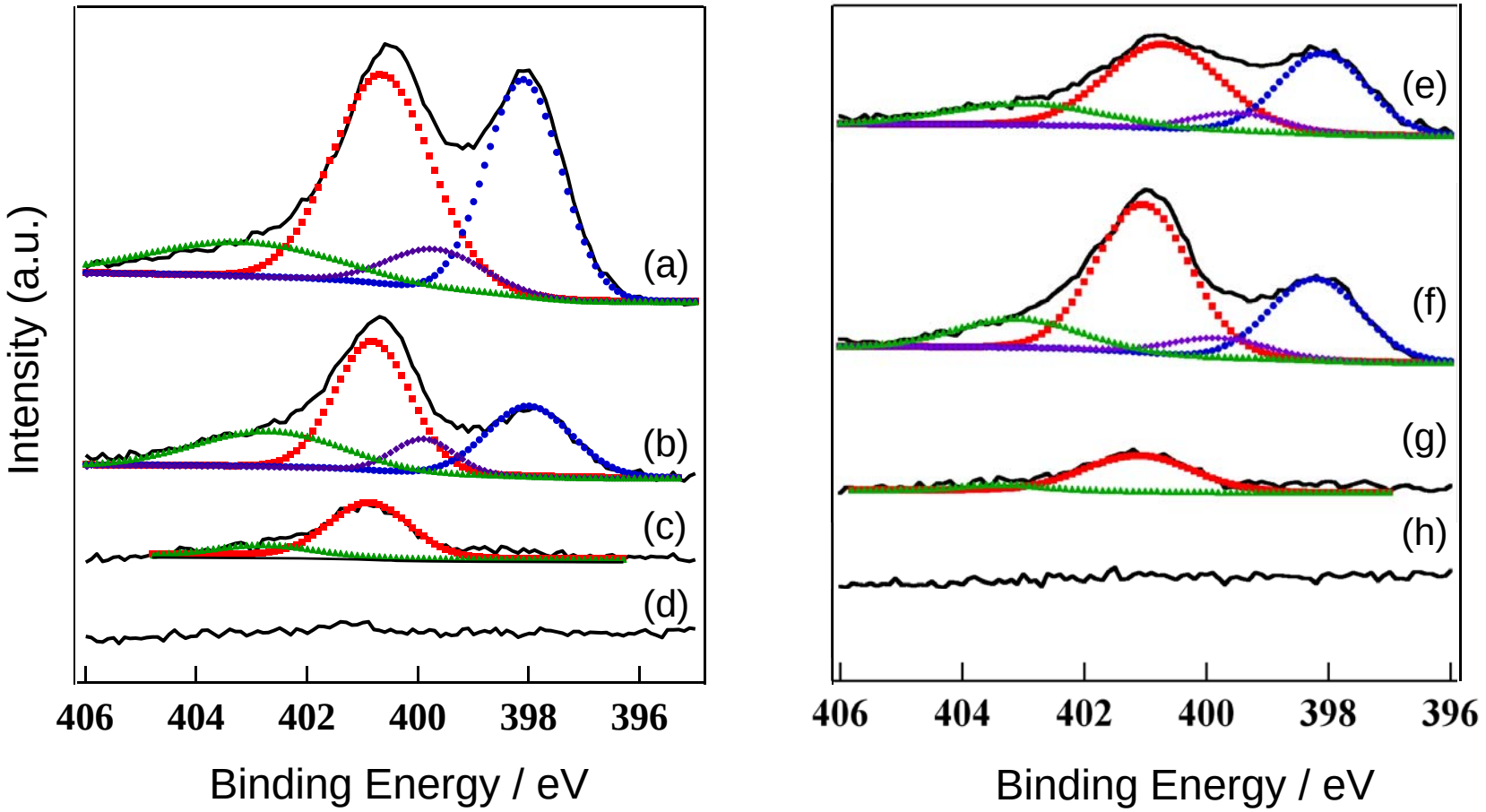

T. Iwazaki et al., Fig. 6

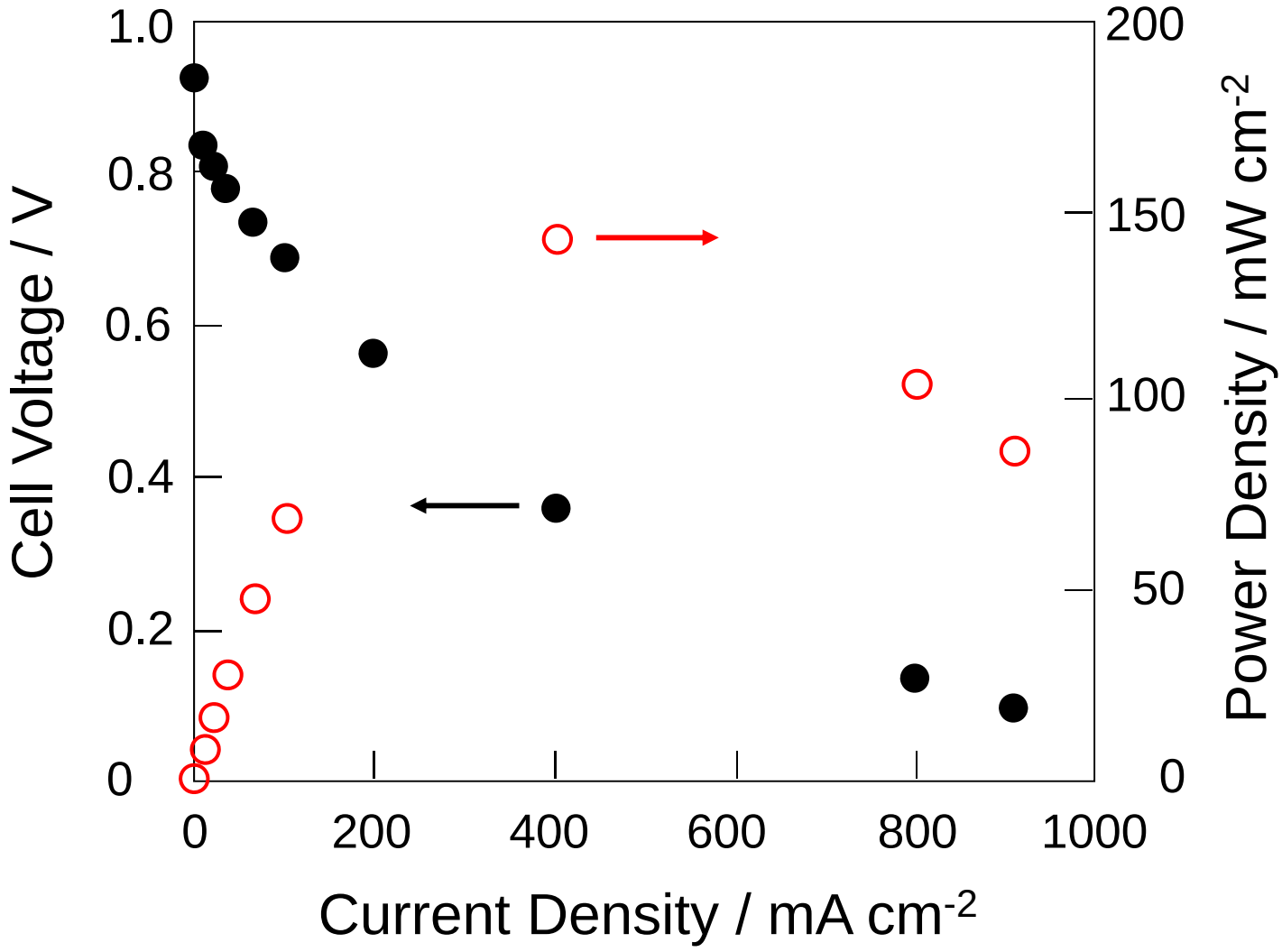

T. Iwazaki et al., Fig. 7

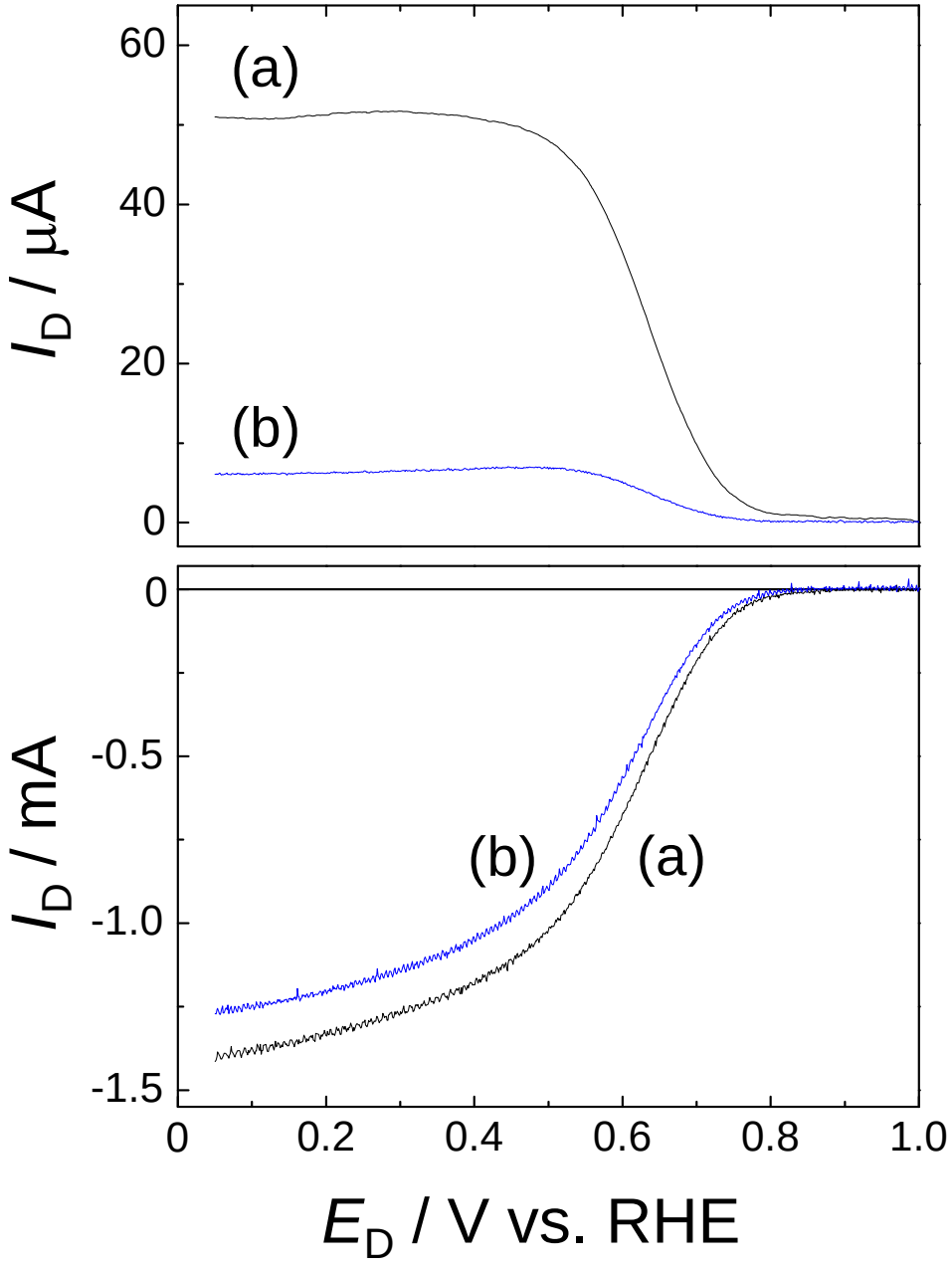

T. Iwazaki et al., Fig. 8

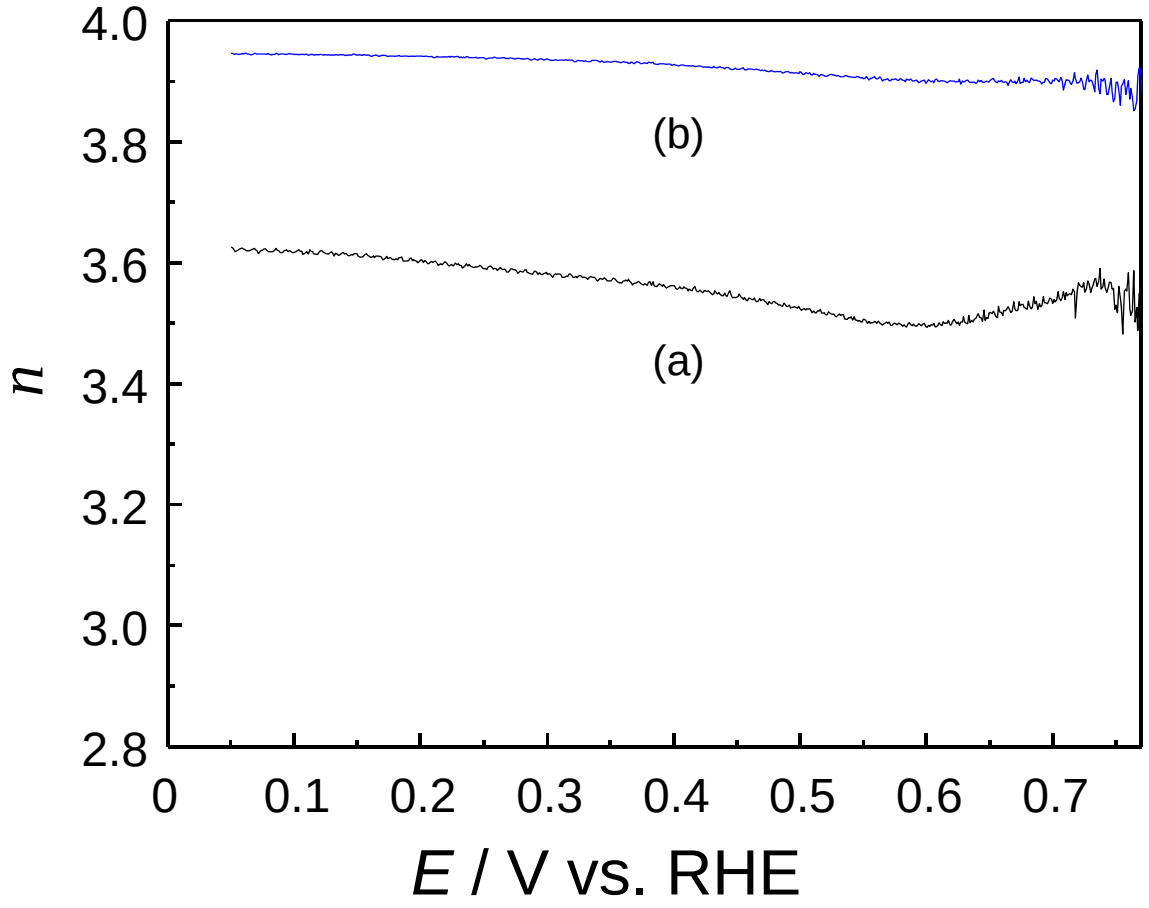

T. Iwazaki et al., Fig. 9

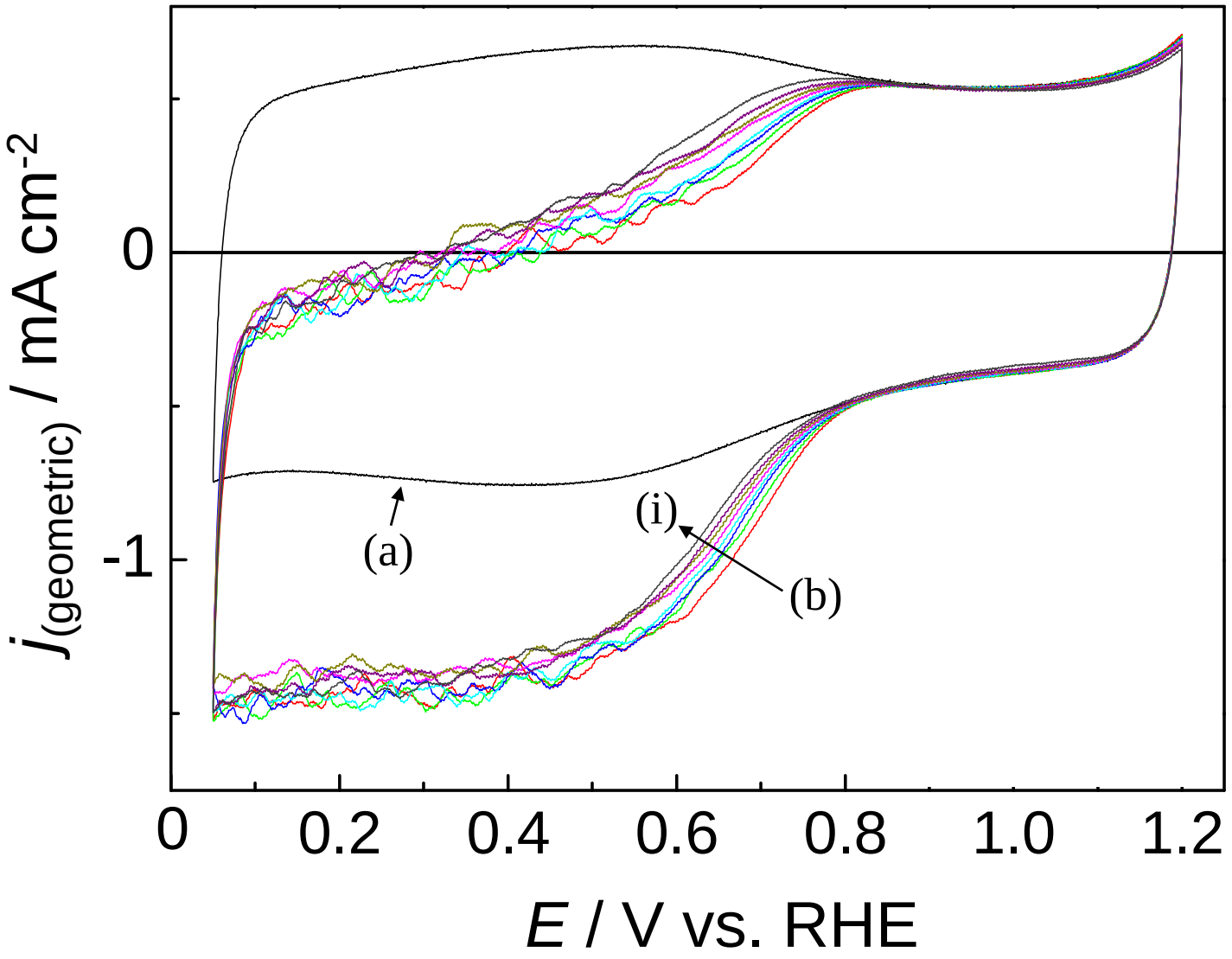

T. Iwazaki et al., Fig. 10

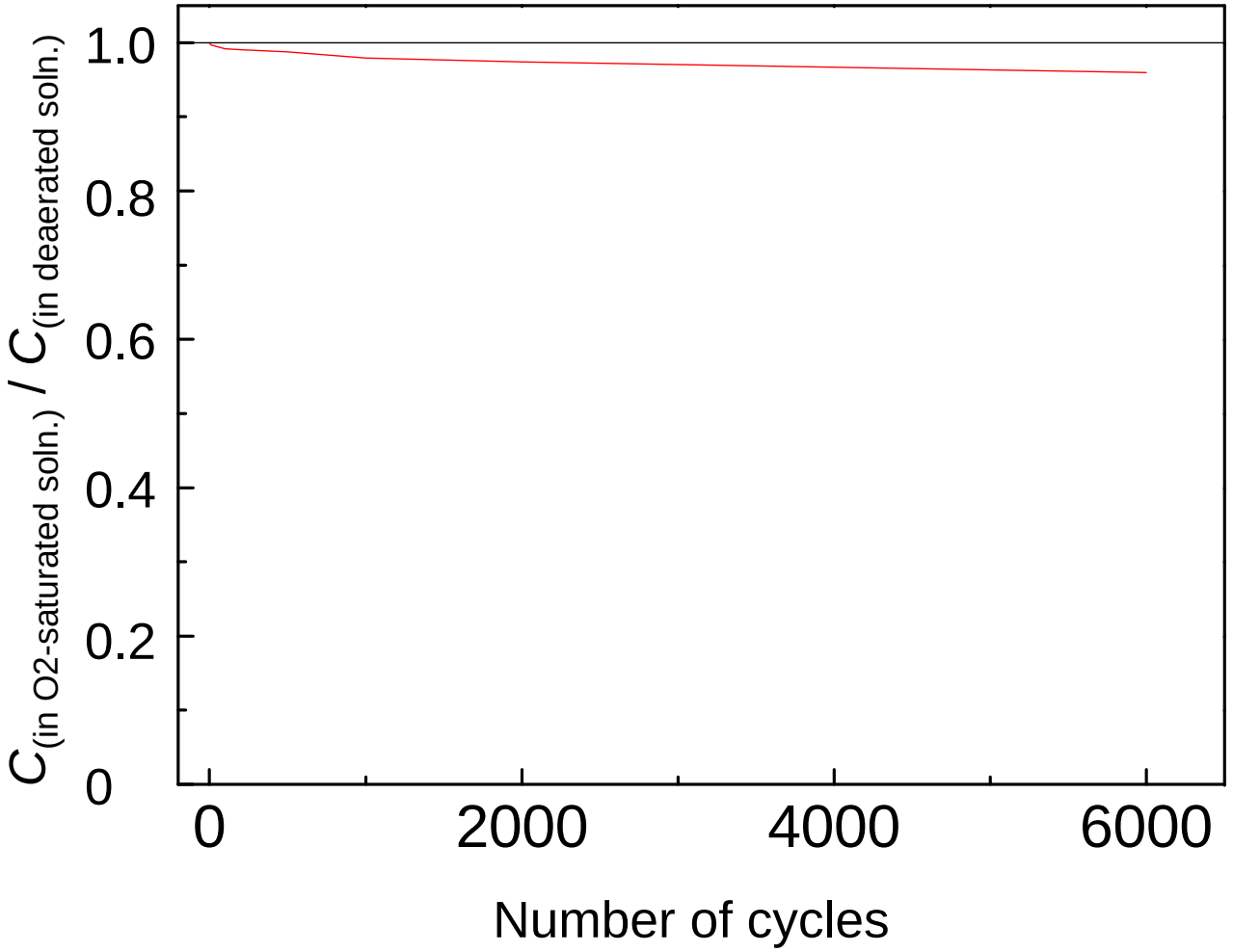

T. Iwazaki et al., Fig. 11

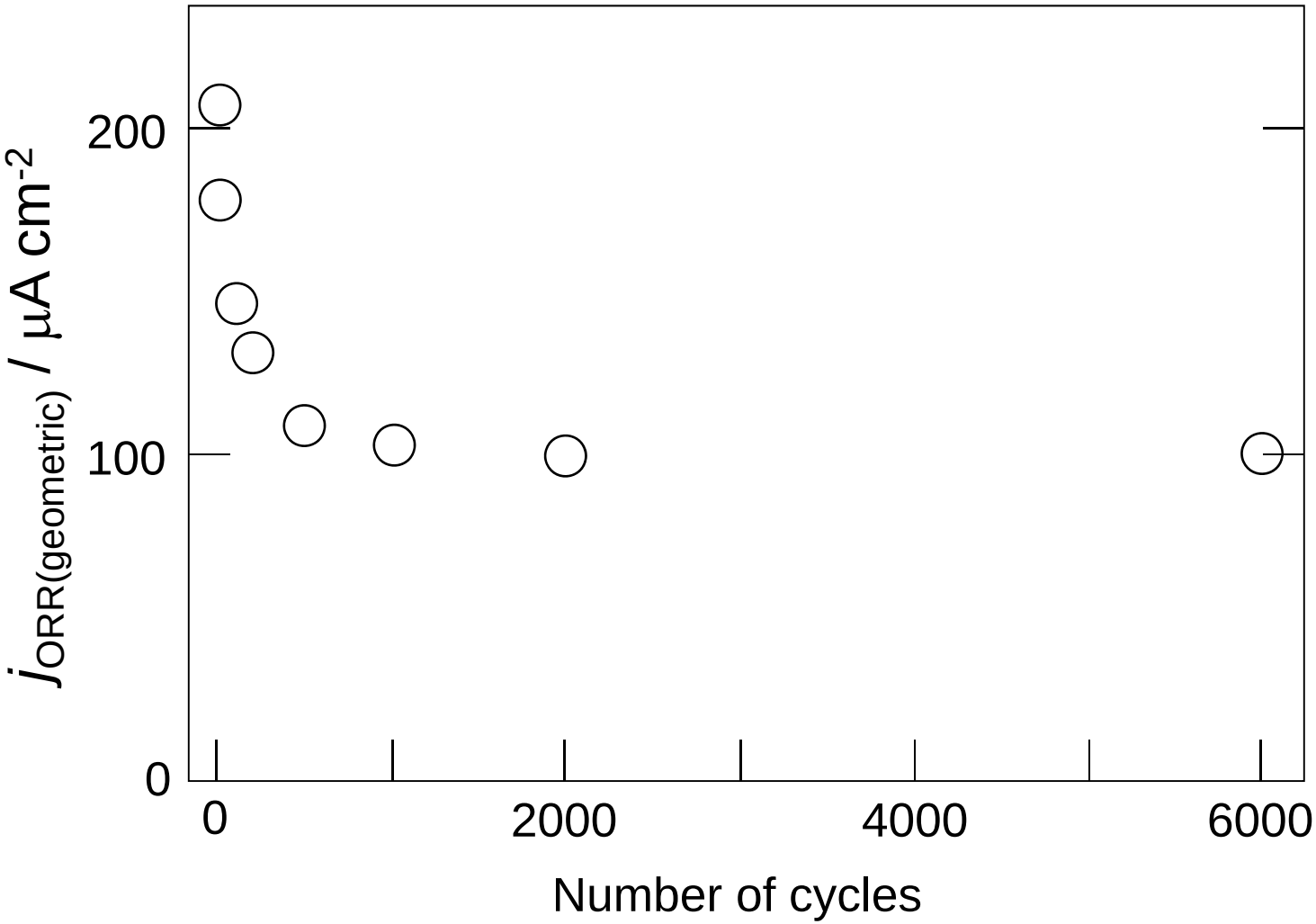

T. Iwazaki et al., Fig. 12